Applied and Environmental Microbiology®

ENZYMOLOGY AND PROTEIN ENGINEERING

Hexachlorobenzene Monooxygenase Substrate Selectivity and Catalysis: Structural and Biochemical Insights

Yuan Guo,[a,b] De-Feng Li,[c] Huining Ji,[a,b] Jianting Zheng,[a,b] Ning-Yi Zhou[a,b]

[a]S a K Lab a M b M ab , Sc L Sc c a B c , S a a T U , S a a C a
[b]J I a a R a c Lab a M ab & D a Sc c , S a a T U , S a a C a
[c]S a K Lab a M b R c , I M b , C Aca Sc c , B , C a

ABSTRACT Hexachlorobenzene (HCB), as one of the persistent organic pollutants (POPs) and a possible human carcinogen, is especially resistant to biodegradation. In this study, HcbA1A3, a distinct flavin-N5-peroxide-utilizing enzyme and the sole known naturally occurring aerobic HCB dechlorinase, was biochemically characterized. Its apparent preference for HCB in binding affinity revealed that HcbA1 could oxidize only HCB rather than less-chlorinated benzenes such as pentachlorobenzene and tetrachlorobenzenes. In addition, the crystal structure of HcbA1 and its complex with flavin mononucleotide (FMN) were resolved, revealing HcbA1 to be a new member of the bacterial luciferase-like family. A much smaller substrate-binding pocket of HcbA1 than is seen with its close homologues suggests a requirement of limited space for catalysis. In the active center, Tyr362 and Asp315 are necessary in maintaining the normal conformation of HcbA1, while Arg311, Arg314, Phe10, Val59, and Met12 are pivotal for the substrate affinity. They are supposed to place HCB at a productive orientation through multiple interactions. His17, with its close contact with the site of oxidation of HCB, probably fixes the target chlorine atom and stabilizes reaction intermediates. The enzymatic characteristics and crystal structures reported here provide new insights into the substrate specificity and catalytic mechanism of HcbA1, which paves the way for its rational engineering and application in the bioremediation of HCB-polluted environments.

IMPORTANCE As an endocrine disrupter and possible carcinogen to human beings, hexachlorobenzene (HCB) is especially resistant to biodegradation, largely due to difficulty in its dechlorination. The lack of knowledge of HCB dechlorinases limits their application in bioremediation. Recently, an HCB monooxygenase, HcbA1A3, representing the only naturally occurring aerobic HCB dechlorinase known so far, was reported. Here, we report its biochemical and structural characterization, providing new insights into its substrate selectivity and catalytic mechanism. This research also increases our understanding of HCB dechlorinases and flavin-N5-peroxide-utilizing enzymes.

KEYWORDS biodegradation, catalytic mechanism, crystal structure, dechlorinase, flavin-N5-peroxide, hexachlorobenzene, monooxygenase

Hexachlorobenzene (HCB; C_6Cl_6) was first introduced in 1945 as a manufactured fungicide. Afterward, it had been widely used in the production of organic solvents, plastics, dyes, pharmaceuticals, and pesticides and in other industries from the mid-1970s (1, 2). Despite having been banned since 1982, HCB is still produced as a by-product from the manufacture of certain chloro-organic chemicals and is subsequently released into the environment. Its residues can be detected in samples of various origins, such as fish, plant, and human blood, indicating the wide distribution of HCB in the environment. Worryingly, chronic exposure of animals and humans to

Citation G Y, L D-F, J H, Z J, Z N-Y. 2021. H ac b a b a c a ca a : c a a b c a . A E M b 87: 01965-20. p :// /10 .1128/AEM.01965-20.

Editor Ma K aa, U Ta

A c p c J Z , @ . c , N -Y Z , @ . c .

Received 10 A 2020
Accepted 14 Oc b 2020
Accepted manuscript posted online 23 Oc b 2020
Published 17 December 2020

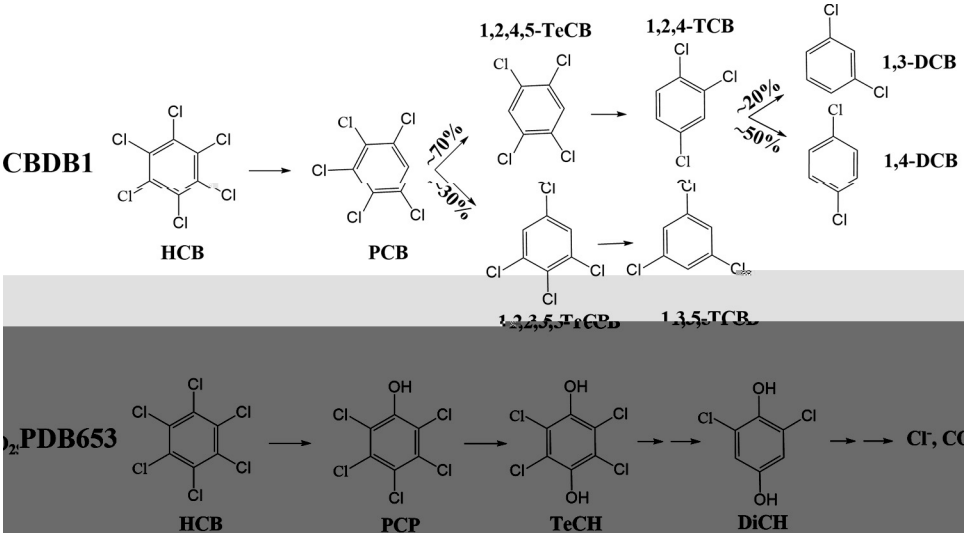

FIG 1 Comparisons of proposed metabolic pathways of HCB in anaerobic strain CBDB1 and aerobic strain PD653. TeCH, tetrachloro- -hydroquinone; DiCH, dichloro- -hydroquinone.

HCB leads to plenty of effects, such as thyroid dysfunctions, porphyria, neurological symptoms, microsomal enzyme induction, tumors of the liver, and immunological disorders (2, 3). Due to its long-term persistence, bioaccumulation, and transport properties, HCB was listed as one of the initial 12 persistent organic pollutants (POPs) by the Stockholm Convention (4, 5).

Microbial degradation is thought to be a promising approach for decontamination of many kinds of pesticides from the environment (6). However, because of high chemical toxicity, inertness, genotoxicity, and lipid solubility, heavily chlorinated benzenes are merely partially degraded at low rates or not at all, with HCB being particularly recalcitrant to biodegradation. Thus, there have been few reports on HCB degradation by bacteria, and the reported studies were mostly conducted under anaerobic conditions (7–11). An oxygen-sensitive strain (CBDB1) capable of reductively dechlorinating HCB was isolated from Saale river sediment, and it has been reported to be one of the most important HCB utilizers in the literature (12). Under aerobic conditions, HCB was shown to be degraded by members of an acclimated microbial community that was dominated by and groups based on 16S rRNA gene analysis (11). sp. strain PD653 was isolated from the soil of a contaminated cabbage field (Ibaraki, Japan) due to its ability to degrade pentachloronitrobenzene (13). Later, it was found to mineralize HCB under aerobic conditions and became the very first (and, to date, only) identified aerobic bacterium capable of mineralizing HCB (13). Surprisingly, PD653 could dechlorinate only HCB among seven halobenzene congeners tested (14). A comparison of proposed HCB metabolic pathways in anaerobic strain CBDB1 and aerobic strain PD653 is shown in Fig. 1.

As dechlorination is the most difficult and rate-limiting step in HCB biodegradation, the characterization of dechlorinases becomes a prerequisite for the in-depth understanding and practical application of HCB biodegradation. Our current knowledge about HCB dechlorinases is very limited in terms of both biochemical characteristics and structural-functional relationships. From the anaerobic bacterium sp. strain CBDB1, CbrA, a chlorobenzene reductive dehalogenase, was identified but not studied further (15). Through rational design, a genetically engineered F87W-Y96F-V247L mutant of CYP101 (P450cam) from was derived for its ability to slowly oxidize HCB to pentachlorophenol (PCP) (16, 17). Mutant F87W-Y96F-L244A-V247L with increased activity toward HCB oxidation was later introduced into a PCP utilizer to construct an engineered HCB degrader (18).

Recently, a unique monooxygenase was isolated from sp. strain PD653 and is the only known naturally occurring enzyme that can aerobically dechlorinate HCB (19). The gene cluster involved in the conversion of HCB to PCP encodes a flavin monooxygenase (HcbA1) and two NAD(P)H:flavin oxidoreductases (HcbA2 and HcbA3). HcbA1 and HcbA3 were proposed to belong to a two-component flavin-diffusible monooxygenase (TC-FDM) system, but their enzymatic characteristics remain unknown.

To provide further insights into the HcbA1A3-catalyzed HCB dechlorination, here we characterized its enzymatic properties and determined the crystal structure of HcbA1. Our report provides a molecular explanation for the high substrate selectivity, insights into the biochemical properties, and also a better understanding of the catalytic mechanism of HcbA1A3. These results will not only broaden and deepen our understanding of HCB monooxygenase HcbA1A3 but also allow comparative studies of structure-function relationships of dechlorinases, TC-FDMs, and flavin-N5-peroxide-utilizing enzymes.

RESULTS

Enzymatic assays. HcbA1 was previously identified as an NADH-dependent and FMN-specific monooxygenase (20). Here, we attempted to isolate FMN from purified HcbA1 using a published method (21), but no flavin was detected, indicating the loose manner of binding of flavin with HcbA1. In an enzymatic experiment, PCP was determined by mass spectrometry to be the only catalytic product transformed from HCB, with a conversion rate of 90.7% ± 3.3% by high-performance liquid chromatography (HPLC).

In a previous study, gene , located between and in the genome of strain PD653, was predicted to encode a flavin reductase. The HCB elimination efficiency shown by cells with , , and (83.0%) was higher than that seen with the cells with and (68.7%) in biotransformation analyses, while no HCB elimination was found for cells with and (19). Here, we expressed and purified HcbA1, HcbA2, and HcbA3 individually in . It turned out that the addition of HcbA2 slightly improved the dechlorinase activity of the HcbA1A3 system and that a system containing HcbA1 and HcbA2 was unable to dechlorinate HCB. Therefore, HcbA2 may be helpful but not essential for HCB monooxygenation. As shown in Fig. 2a, the optimal molar ratio of HcbA1 to HcbA3 was 90:1 for our reaction system. That means that it requires large amount of HcbA1 to achieve optimal efficiency when the molar amount of HcbA3 is constant. Therefore, such a high molar ratio indicates their low coupling efficiency; the oxygenase activity of HcbA1 is weak compared with the high flavin-reducing activity of HcbA3. In terms of functional evolution, this couple has yet to reach its optimal state. In a time course experiment (Fig. 2b), HCB consumption and reaction duration showed linearity over the first 10 min. The optimal temperature and pH of HCB oxidation catalyzed by HcbA1A3 were 37.5°C and pH 8 (in HEPES buffer), respectively (Fig. 2c and d). The specific activity, Michaelis constant , and catalytic constant $_{cat}$ of HcbA1A3 for HCB were 8.26 ± 0.67 μmol/min·g, 20.17 ± 1.61 μM, and 0.41 ± 0.03 min^{-1}, respectively.

Substrate selectivity. Less-chlorinated benzenes are generally considered to be more biodegradable than HCB (22), and yet sp. strain PD653 showed an extremely narrow substrate range among different halogenated benzenes and halogenated nitrobenzenes (14). Correspondingly, here, investigating the substrate range of HcbA1A3, no product was detected using chlorobenzene (CB), 1,2-dichlorobenzene (1,2-DCB), 1,4-dichlorobenzene (1,4-DCB), 1,2,3-trichlorobenzene (1,2,3-TCB), 1,3,5-trichlorobenzene (1,3,5-TCB), 1,2,3,4-tetrachlorobenzene (1,2,3,4-TeCB), 1,2,4,5-tetrachlorobenzene (1,2,4,5-TeCB), 1,2,3,5-tetrachlorobenzene (1,2,3,5-TeCB), pentachlorobenzene (PCB), or 1,3,5-tribromobenzene as the substrate, confirming its high substrate specificity. Thus, the following two alternative hypotheses were proposed: the less-chlorinated benzenes were unable to bind into HcbA1, or they were unable to be oxidized after a successful binding. To address this issue, interaction analyses of HcbA1 and the substrates were conducted using

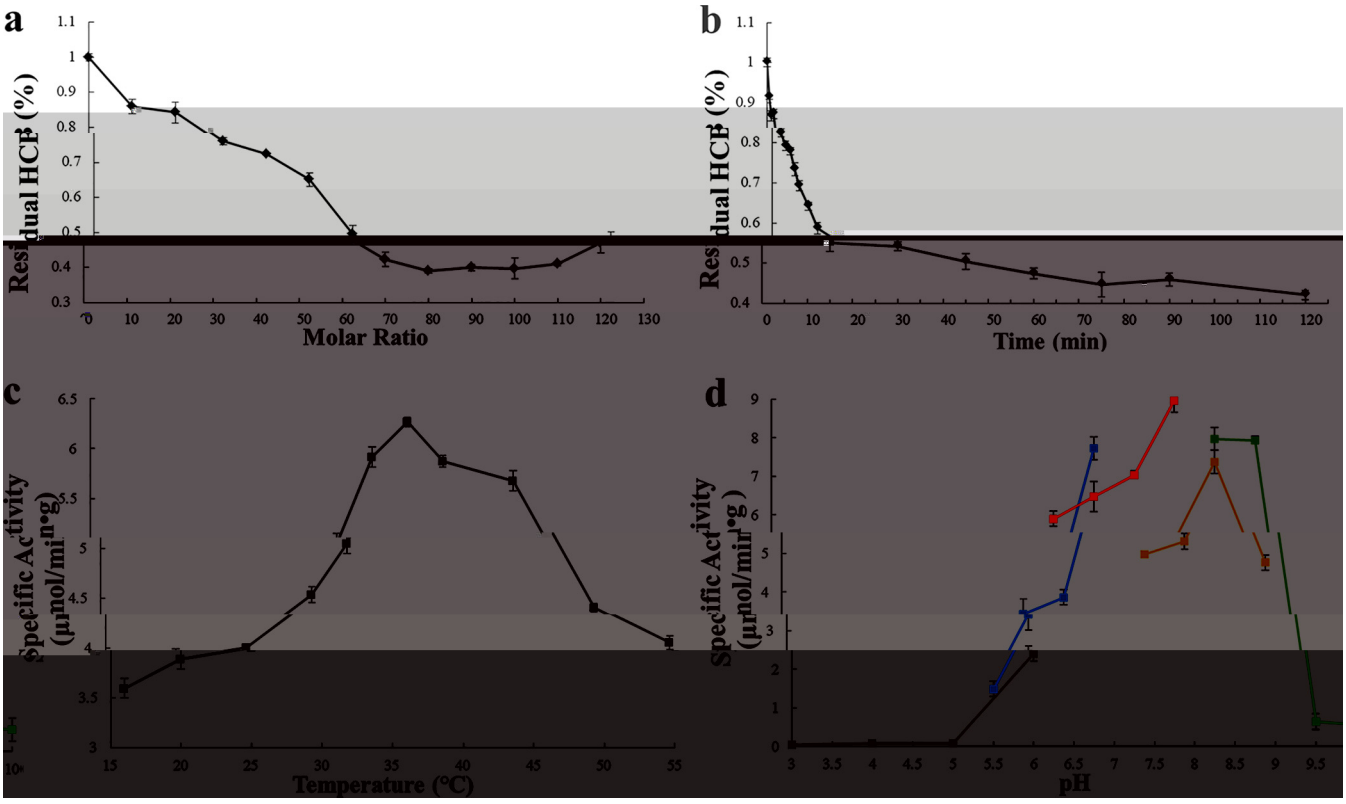

FIG 2 Biochemical characterization of HcbA1A3. (a) Effect of molar ratios of HcbA1 to HcbA3 on hexachlorobenzene (HCB) consumption. (b) Effect of reaction duration on HCB consumption. The ordinate shows the percentages of residual HCB with respect to the initial HCB level. (c) Effect of temperature on the enzyme activity of HcbA1A3. (d) Effect of pH on the enzyme activity of HcbA1A3. The gray line represents citrate buffer, the blue line represents MES buffer, the red line represents HEPES buffer, the orange line represents Tris-HCl buffer, and the green line represents glycine buffer.

ForteBio Octet. HCB showed a much higher affinity (an equilibrium dissociation constant [K_D] of 1×10^{-12} M) than PCB, 1,2,3,4-TeCB, and 1,2,4,5-TeCB (2.1×10^{-4} M, 1.5×10^{-4} M, and 1.4×10^{-4} M, respectively) for the HcbA1-FMN complex (see Fig. 5a). Therefore, the difficulties in binding probably prevented less-chlorinated benzenes from being oxidized.

Overall structure of HcbA1. The HcbA1 crystal belongs to space group 222_1 and has unit cell parameters of a = 112.1 Å, b = 139.3 Å, and c = 169.0 Å, with a solvent content of 63.27%. HcbA1 is present in the asymmetric unit as a homodimer (Fig. 3a), which is consistent with the state determined in solution by gel filtration chromatography. The diffraction data and refinement statistics are listed in Table 1.

According to the crystal structure, apo-HcbA1 is essentially composed of a $(\beta/\alpha)_8$ barrel (TIM fold barrel) (23), arranged as β1-α1-β2-α3-β3-α4-β4-α6-β5-α7-β6-α8-β7-α13-β9-α14. Therefore, HcbA1 belongs to the luciferase-like superfamily (24). One subunit of HcbA1 contains 15 α-helices, 9 β-strands, and 3 η-helices. In addition to the prototypical TIM-barrel structure, there are five additional insertions (AI1 to AI5) and a C-terminal extension (positions 413 to 451) as follows: AI1 (residues 13 to 35), AI2 (residues 58 to 84), AI3 (residues 136 to 155), AI4 (residues 175 to 222), and AI5 (residues 286 to 369) (Fig. 3b). AI4 is a two-hairpin region and is the most extensive of the five additional insertions. The two hairpins clearly protrude from the protein core, and one of them extends into the neighboring subunit. Thus, AI4 contributes to the dimerization stability of HcbA1. AI5 covers the cavity of the barrel fold, with a relatively high level of flexibility. This region probably acts as a "gate" conducting a conformational change between an "open" and a "closed" form during the substrate-binding process as other TC-FDMs do (25, 26). The C-terminal extension contains two short helices (η3 and α15), of which η3 blocks the N terminus of the β-barrel. The four insertions (except for AI4),

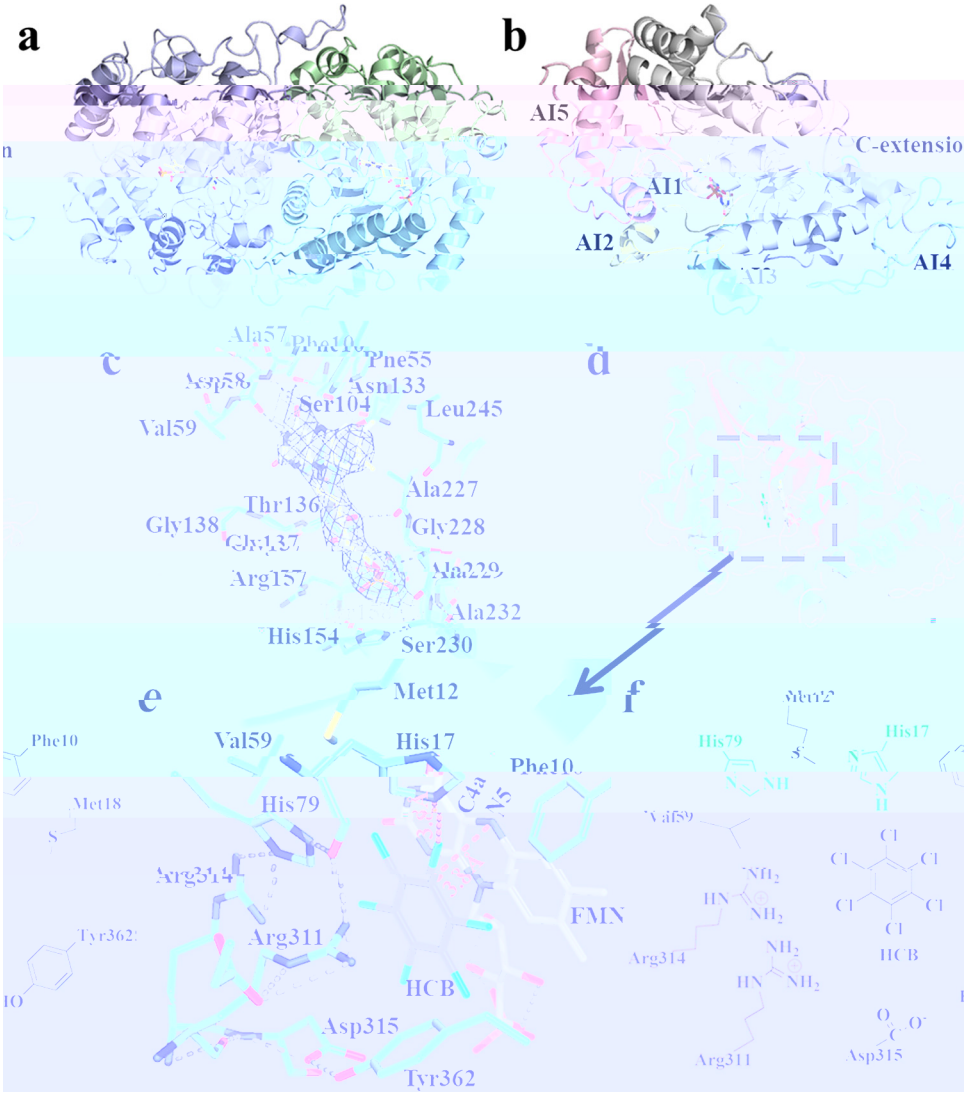

FIG 3 The structure of HcbA1. (a) Overall structure of the HcbA1 dimer. Each subunit is shown in a different color (chain A, blue; chain B, green). (b) Five insertions (AI1 to AI5) of the HcbA1 subunit. AI1, AI2, AI3, AI4, AI5, and the C-extension are colored in wheat, yellow, green, cyan, pink, and blue, respectively. (c) F_o-F_c difference map calculated with the ligand omitted, contoured at 2.0 σ around modeled FMN. The hydrogen bond interactions of FMN with surrounding residues are shown as gray dashes. (d) The surface of HcbA1 features a substrate and flavin binding pocket. (e) The structure model of HcbA1·FMN docked with hexachlorobenzene (HCB). The orange dashed lines show the distances from the site of oxidation to the reactive N5 of FMN and from the target chlorine atom to the Nε2 of His17. The hydrogen bond network of the active center is shown as gray dashes. (f) A schematic of the active site of HcbA1.

together with the C terminus of the β-barrel, are involved in the constitution of active site.

The approximate dimensions of the HcbA1 homodimer are 79 × 55 × 47 Å^3. Calculated by the PISA server (27), approximately 15% of the total solvent-accessible area is buried at the subunit interface. Helices α3 and α4 are the most important secondary structures in this interaction. The dimerization between the two subunits is through hydrophobic interactions, hydrogen bonds, and salt bridges. In each monomer, 25 amino acid residues are involved in hydrogen bond interactions, distributed in α4, AI1, AI2, AI3, and AI4. Asp58 (in AI2) forms a salt bridge with Lys117 (in α4) of a neighboring subunit, which is conserved and commonly exists in its homologues. There are some conserved residues in areas involved in the dimerization or tetramerization of the luciferase-like family (see Table S1 in the supplemental material), suggesting that dimerization or tetramerization is essential for their functions.

TABLE 1 Data collection and refinement statistics

Parameter	Value(s)	
	APO-HCBA1	HCBA1·fMN

FMN binding. The crystal structure of the HcbA1-FMN complex was determined at a resolution of 3.2 Å. The electron density map of FMN and its hydrogen-bonding interactions with surrounding residues are shown in Fig. 3c. The overall structure of the HcbA1-FMN complex is similar to that of the ligand-free form, with a root mean square deviation (RMSD) of 0.299 Å for Cα atoms. The location and manner of binding of FMN in HcbA1 are similar to those of other luciferase-like family members, such as long-chain alkane monooxygenase LadA (28), uracil monooxygenase RutA (29), and bacterial luciferase LuxA/B (30). The flavin ring lies in the C terminus of the β-barrel with its plane almost perpendicular to the β-sheets of the barrel. Its face faces the barrel and the face is exposed to solvent. Therefore, O_2 activation probably occurs on the side whereas the substrate binds on the side (Fig. 3c). Both hydrophobic and hydrogen bond interactions are involved in the binding of FMN. The N3 atom of FMN engages in hydrogen bonding with the backbone oxygen of Asp58. The O4 atom forms hydrogen bonds with the nitrogen atom of Asp58 and the hydroxyl group of Ser104. The dimethylbenzene fragment performs extensive hydrophobic interactions with a cluster of hydrophobic residues, including Phe10, Phe55, Val135, Ala227, Ala229, and Leu245. The imidazolyl of His154, the phenolic hydroxyl of Tyr158, and the hydroxyl of Ser230, as well as the nitrogen atom of Ala229, are all associated with fixing the phosphate group of FMN.

Substrate binding. Despite substantial efforts, our attempt at cocrystallization with HCB was not successful, which could have been a consequence of the low ligand solubility. To gain preliminary knowledge on substrate binding and understand the dechlorination mechanism, we built a structural model of the HcbA1·FMN·HCB ternary complex by docking HCB into the HcbA1·FMN crystal structure (Fig. 3d and e). The eight poses of HCB adopted almost the same binding mode, with only negligible differences (Table S2), and the first one listed in Table S2 was selected for analysis.

The HcbA1·FMN binary complex defines a cavity at the / face of FMN, which would accommodate a substrate. Residues Phe10, Met12, Val59, and Met18 constitute a hydrophobic environment, which is pivotal for all enzymes using aromatic substrates. Four basic residues, Arg311, Arg314, His79, and His17, are located very close to HCB. The guanidine groups of Arg311 and Arg314 as well as the imidazole group of His79 face one side of the aromatic ring of HCB, while His17 locates above HCB with close contact with the N5 atom of FMN (Fig. 3e).

A tightly connected hydrogen bond network, consisting of His17, His79, Arg311, Arg314, Asp315, Tyr362, Met18, and Asp20, was observed in the active center. In this network, Asp315 engages in hydrogen bonding with Tyr362, and they are located closely below HCB and at the entrance of the substrate pocket (Fig. 3e). Moreover, this hydrogen bond is crucial for linking α10 and β8 and thus is proposed to be important for maintaining the conformation of the active center.

Identification of oxidation site. Identification of which carbon atom in HCB was the site of oxidation can facilitate our understanding of the roles of the key residues as well as of the reaction mechanism. In accordance with the distances to N5 and C4a of FMN ($N5_{FMN}$ and $C4a_{FMN}$), two carbon atoms of HCB, labeled C1 and C2 in Fig. 3e, were chosen as candidates for nucleophilic attack. In the HcbA1·FMN·HCB model, the distances of C1 to $N5_{FMN}$ and C1 to $C4a_{FMN}$ are 3.8 Å and 4.1 Å, while the distances of C2 to $N5_{FMN}$ and C2 to $C4a_{FMN}$ are 4.1 Å and 3.8 Å, respectively. Thus, C1 has a shorter distance with $N5_{FMN}$ than C2 does. In addition, a molecular dynamic (MD) simulation was performed on the structure model of HcbA1·FMN·HCB. The distances of C1 to $N5_{FMN}$, C1 to $C4a_{FMN}$, Cl1 to $N5_{FMN}$, and Cl1 to $C4a_{FMN}$, as well as C2 to $N5_{FMN}$, C2 to $C4a_{FMN}$, Cl2 to $N5_{FMN}$, and Cl2 to $C4a_{FMN}$, during 50 ns to 150 ns of MD were then calculated (Fig. 4). C1 was found to show shorter distances with both $N5_{FMN}$ and $C4a_{FMN}$ (average values of 4.57 Å and 4.43 Å, respectively) than were measured for C2 (4.72 Å and 4.59 Å), indicating that C1 is more likely to be the site of oxidation.

Mutagenesis of key residues. Through site-directed mutagenesis, the functions of some residues that are important for HcbA1's activity were revealed (Table 2; see also Fig. 5b). Hydrophobic residues Phe10, Val59, and Met12 sit in close proximity to both FMN and HCB. The mutations of the aforementioned residues largely abolished the enzymatic activities, accompanied by a sharp decrease of the binding affinity for HCB (with increased / values). Considering that these residues may relate not only to the binding of HCB but also to the binding of FMN, it was not entirely clear whether these residues affected the substrate affinity directly or indirectly. Tyr362 and Asp315 represent a pair of hydrogen-bonded residues that are supposed to maintain the conformation of the active center. Their mutants Y362S, Y362F, and D315A were expressed insolubly, confirming their necessity for maintaining the protein folding. Mutations R311L, R314L, and H79A were entirely inactive, without significant conformational change (confirmed by circular dichroism [CD]), indicating the importance of these residues for enzyme activity. In addition, their / values for HCB were all significantly increased compared with the values measured for the wild type, which thereby underlines the necessity of Arg311, Arg314, and His79 for substrate binding. However, knowledge of their functions in catalytic processes remains elusive. The Nε2 atom of His17 sits closely above the target chlorine atom of HCB with a distance of 3.8 Å (Fig. 3e). Enzyme activity was largely abolished in variant H17A (with 31% of the specific activity of the wild type) and was accompanied by a sharp decrease in the binding affinity for HCB.

DISCUSSION

Protein-substrate molecular interactions. Although HCB cannot be engaged in hydrogen bonds, the geometry of HcbA1's active center places HCB at a productive location and orientation. The possible interactions are discussed as follows. (i) A hydrophobic environment is the foundation of a substrate-binding pocket for aromatic compounds, as confirmed by the mutagenesis results from analysis of F10A, V59A, and M12A. (ii) Arg311 and Arg314 have been proven to be necessary for binding HCB. The

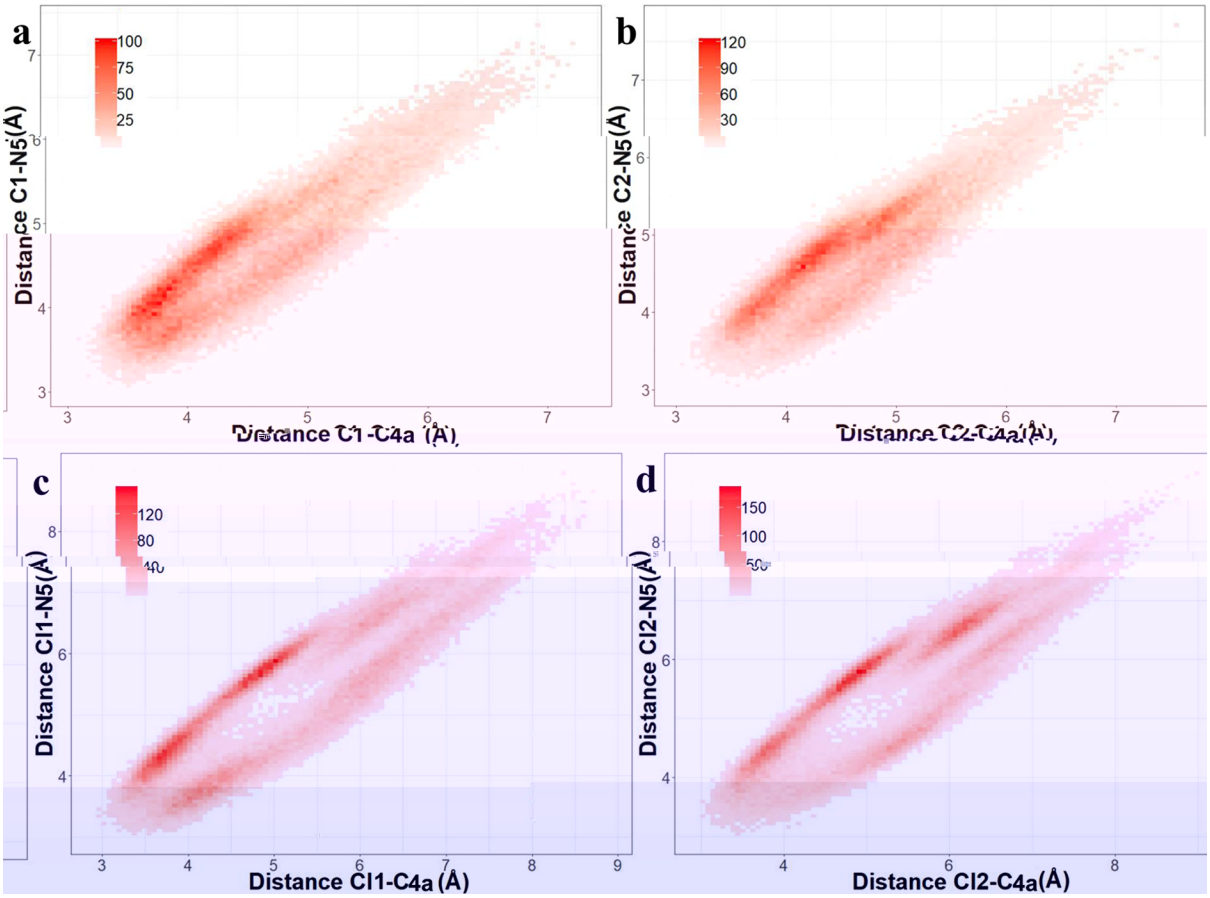

FIG 4 The interatomic distances measured during molecular dynamics (MD) simulations of HcbA1·FMN·HCB. During the MD simulations, C1 and Cl1 of HCB showed shorter distances with respect to N5/C4a of FMN than with those of C2 and Cl2. (a) Distances between C1 and N5/C4a. (b) Distances between C2 and N5/C4a. (c) Distances between Cl1 and N5/C4a. (d) Distances between Cl2 and N5/C4a. The distances shown here represent the statistics for 50 to 150 ns during MD.

positively charged guanidinium groups can have both an electrostatic attraction for the chlorine atoms and a cation-π interaction with the aryl of HCB (31, 32). (iii) The aromatic ring of Tyr362 and the imidazole ring of His79, as well as the isoalloxazine ring of FMN, may form π-π interactions with the aryl of HCB. (iv) Because of the unique electronic properties of halogens bound to an aryl, the halogens form halogen bonds with nucleophiles (31, 33). Therefore, Nε2 of His17 is suggested to help fix the target chlorine

TABLE 2 Specific activities and binding affinities for HCB of wild-type HcbA1 and its mutants

Category	Protein	Sp act (μmol/min·g)	K_D (M) for HCB
Wild type	HcbA1	8.26 ± 0.67	1.0×10^{-12}
Active mutant	H17A	2.55 ± 0.19	2.2×10^{-7}
	M12A	4.87 ± 0.54	1.8×10^{-7}
Inactive mutant	R311L		1.8×10^{-5}
	R314L		4.5×10^{-5}
	H79A		2.0×10^{-5}
	V59A		8.6×10^{-5}
	F10A		2.1×10^{-4}
Insoluble mutant	Y362S		
	Y362F		
	D315A		

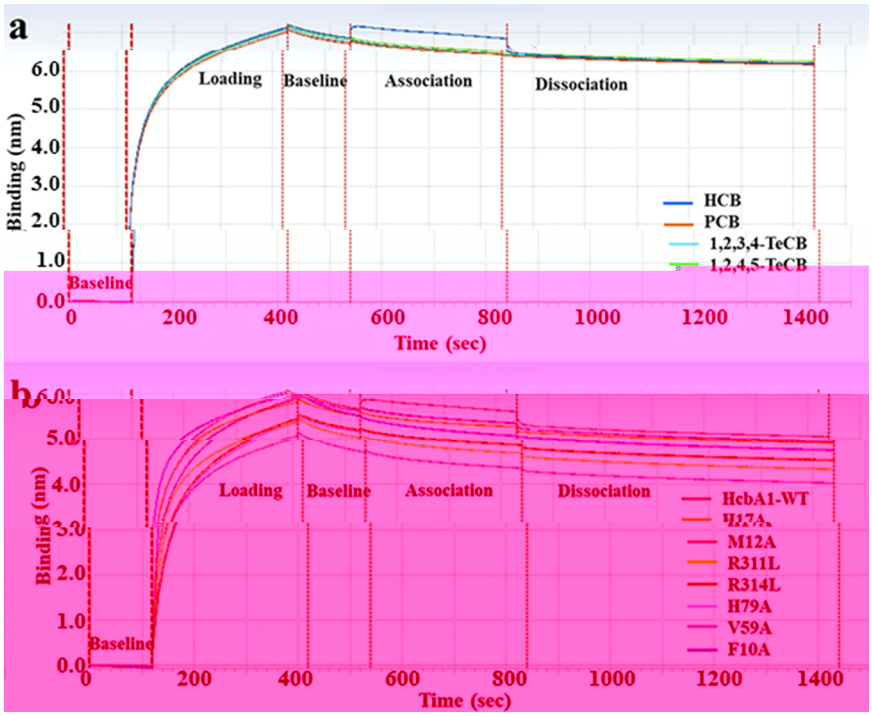

FIG 5 Substrate-enzyme binding affinity analysis by ForteBio Octet. (a) HCB, PCB, 1,2,3,4-TeCB, and 1,2,4,5-TeCB were used to test their binding affinities with wild-type HcbA1. (b) HCB was used to test its binding affinities with wild-type HcbA1, as well with as its mutants H17A, M12A, R311L, R314L, H79A, V59A, and F10A.

atom to facilitate the oxidation of target site. (v) A halogen-π interaction between Phe10 and the target chlorine atom, similarly to the geometry of the Br-Phe interaction in nitric oxide synthase (PDB entry 1D0C) (32, 34), may be indispensable for the accurate orientation of HCB.

From our results, HcbA1 showed high selectivity for HCB and significantly weaker capacities to bind less-chlorinated benzenes. In comparison with HCB, the absence of a chlorine atom in PCB had an obvious effect on the substrate binding or orientation. Therefore, we suppose that PCB is unable to be stably coordinated by the active center because of the absence of an interaction between His17 (as well as Phe10, possibly) and the target chlorine atom (Fig. 3e). Likewise, TeCBs, TCBs, and DCBs would break more enzyme-chlorine interactions, such as Cl with Arg311 and Cl with Arg314. However, experimental data are needed to corroborate the hypothesis.

Comparison with homologues. An evolutionary tree of HcbA1 that includes known members of bacterial luciferase-like family was constructed to investigate the relationship between HcbA1 and related proteins (see Fig. S1 in the supplemental material). To understand their structural similarity, a search was conducted using the DALI server (35). LadA was identified as the closest structural homologue to HcbA1 in the RCSB Protein Data Bank, which is reflected by an RMSD of 1.7 Å for Cα atoms. HcbA1 shows 38% amino acid sequence identity with LadA and 37% to 29% sequence identities with the other proteins listed in Table S1 in the supplemental material.

HcbA1 shows the smallest pocket compared with its homologues listed in Table S1, which is reflected in both the mouth opening area and the pocket volume (350 Å^2 and 3,107 Å^3, respectively, as calculated by CASTp [36]). The homologues have mouth opening areas of 511 to 1,118 Å^2 and pocket volumes of 3,819 to 8,157 Å^3 (Table S1). This demonstrates a limited space of the substrate pocket in HcbA1, which is mainly determined by its AI5 segment, especially residues 305 to 363. In HcbA1, α10 (where Arg311, Arg314, and Asp315 are located) and α12 (where Tyr362 is located) constitute important parts of the substrate pocket. In contrast, in LadA, DmoA, RcaE, and BdsA,

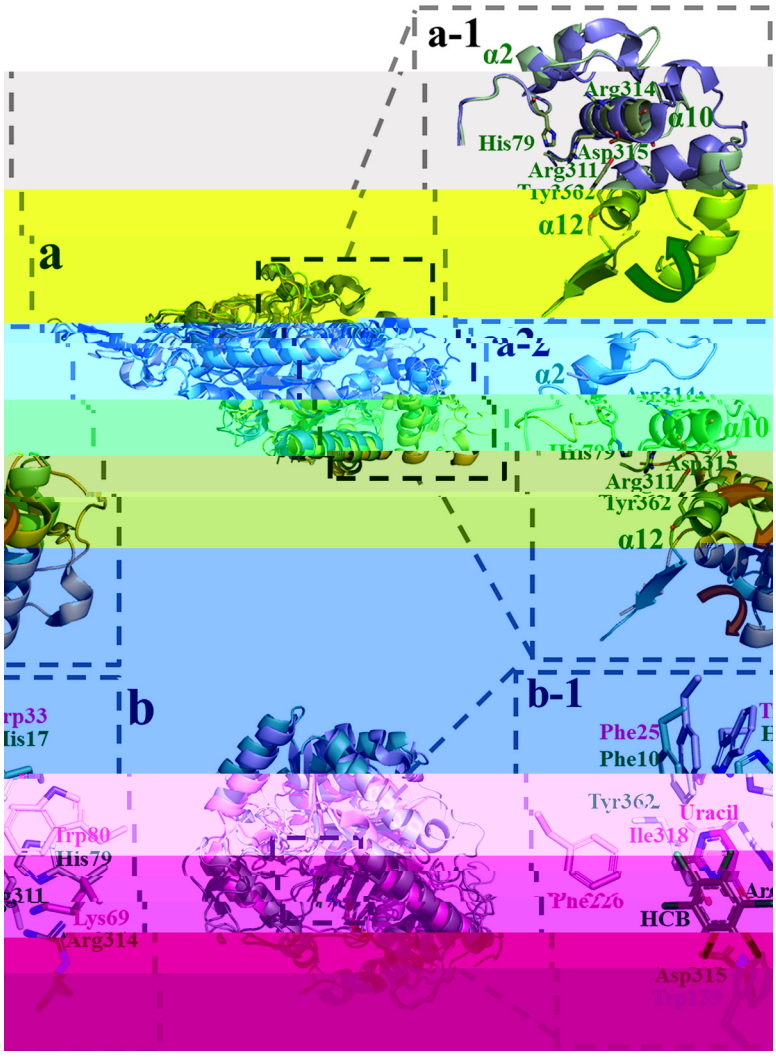

FIG 6 Structural comparison of HcbA1 and its homologues. (a) Superposition of HcbA1 (green), LadA (blue), and EmoA (orange). (a-1) Comparison between HcbA1 (green) and LadA (blue) in segments AI2 and AI5. (a-2) Comparison between HcbA1 (green) and EmoA (orange) in segments AI2 and AI5. (b) Superposition of HcbA1 (green) and RutA (pink). (b-1) Comparison between the substrate-binding pockets of HcbA1 (green) and RutA (pink).

α12 is pushed away from the active center (Fig. 6, panel a-1). Moreover, both α10 and α12 are pushed far away in MoxC, NmoA, and EmoA (Fig. 6, panel a-2). The different locations of these two α-helices result in significant differences in the mouth opening areas and pocket volumes. Another difference was observed in AI2, which has only one α-helix (α2), where His79 is located. The location of α2 in LadA, DmoA, RcaE, and BdsA is the same as in HcbA1 (Fig. 6, panel a-1). The α2 helices of MoxC and NmoA, however, are perpendicular to that of HcbA1, and no α-helix at the corresponding location was observed in the AI2 of EmoA (Fig. 6, panel a-2). These obvious structural differences are likely associated with their various substrate specificities and evolutionary origins. Considering that the presence of six identical substituents of HCB is unfavorable for its accurate binding, a small-sized substrate pocket in HcbA1 may be necessary because of its facilitating HCB's correct location and orientation.

Comparison with the HCB-dechlorinating mutant of CYP101. Before the characterization of HcbA1, the only reported example of aerobic HCB dechlorinase was a genetically engineered cytochrome P450cam: the F87W/Y96F/V247L mutant of CYP101 from . Wild-type CYP101 can catalyze slow oxidation of dichloro-

benzenes and trichlorobenzenes, producing corresponding chlorophenols, but no products were detected for heavily chlorinated benzenes. A Y96F mutant with increased active-site hydrophobicity was found to be able to slowly oxidize PCB and HCB to PCP (16). Therefore, unlike HcbA1's apparent substrate selectivity for HCB, the F87W/Y96F/V247L mutant of CYP101 showed extended activities on many substrates, including 1,2-DCB, 1,3-DCB, 1,4-DCB, 1,3,5-DCB, 1,2,4,5-TeCB, PCB, and HCB. In terms of catalytic mechanism, CYP101 is also significantly different from the flavin-dependent HcbA1. The P450 cytochromes are a large family of heme-dependent monooxygenases and catalyze the oxidative transformation of a great variety of endogeneous and exogeneous organic compounds, ranging from alkanes to polyaromatic compounds (37). P450 cytochromes generate a highly oxidizing oxy-ferryl porphyrin cation radical intermediate through activating dioxygen with two electrons from NAD(P)H and two protons. In contrast, for HcbA1, reaction of reduced flavin with oxygen generates a flavin C4a-(hydro)peroxide that reacts with electrophilic or nucleophilic substrates. In addition, the residues in the substrate pocket of the F87W/Y96F/V247L mutant, including Phe96, Phe98, Trp87, Leu247, Val295, Val396, and Leu244, are dominantly hydrophobic, except for two hydrophilic residues, Thr252 and Asp297. Given that the hydrophobicity-increasing mutation Y96F conferred the ability of oxidation of HCB to CYP101 (16), it is supposed that the CYP101 mutant binds HCB mainly through hydrophobic interactions. In contrast, hydrophilic residues make up a large proportion in HcbA1's substrate pocket and both hydrophobic interaction and electrostatic interaction are necessary for the HcbA1-HCB interaction.

Comparison with the flavin-N5-peroxide-utilizing RutA. In the past few years, the formation of a flavin-N5-oxide intermediate was proven by analysis of the reactions catalyzed by HcbA1 (20), EncM (polyketide oxidase) (38, 39), DszA (dibenzothiophene sulfone monooxygenase) (40), and RutA (amide monooxygenase) (41, 42). Recently, in RutA, data showed that flavin-N5-peroxide might perform as a soft α-nucleophile for catalysis instead of the prevalent flavin-C4a-peroxide that was exclusively taken for an electrophile/nucleophile in flavin-dependent monooxygenases (29). Despite sharing only 20% identity in their amino acid sequences, RutA and HcbA1 resemble each other structurally to a certain extent. Their overall protein folds are similar, with FMN molecules positioned in the same fashion in both (Fig. 6b). The most important oxygen reactivity residues in RutA are Thr105 and Asn134, which stabilize the transient superoxide radical via strong hydrogen bonds. The consensuses of these two residues are Ser104 and Asn133 in HcbA1. Other residues involved in oxygen reactivity are also highly conserved between RutA and HcbA1. On the one hand, the residues in RutA and HcbA1 have some features in common (Fig. 6, panel b-1). Hydrophobic residues Phe25, Met67, and Met320 of RutA are located at positions corresponding to those of Phe10, Met12, and Met18 of HcbA1. The positions of His17 and His79 in HcbA1 are taken by Trp33 and Trp80 in RutA. Histidine and tryptophan both contain a nitrogen heterocyclic ring, and their nitrogen atoms may be directly related to the substrate binding and catalysis. On the other hand, these two enzymes have many differences as follows (Fig. 6, panel b-1). The substrate-binding pocket of RutA is much more hydrophobic than HcbA1, since there is only one hydrophilic residue, Lys69. Another obvious difference that was observed was that Phe226 and Trp139 of RutA have no homologue residues in the corresponding positions of HcbA1. They have high levels of steric hindrance and extend toward the entrance of the substrate-binding pocket. This possibly facilitates the stabilization of a smaller substrate, uracil.

Implications for the catalytic mechanism. On the basis of previous results and our current studies, the catalytic mechanism of HcbA1 (Fig. S2) is summarized below and as follows. (i) $FMNH_2$, supplied by HcbA3, binds to HcbA1. (ii) In RutA, substrate binding promotes N5 oxygenation formation (29). Similarly, it was deduced that, first, HCB binds to the HcbA1-$FMNH_2$ complex, and then $FMNH_2$ accepts O_2 at the N5 position, producing a flavin-N5-peroxide. And this N5 oxygenation is facilitated by Ser104, Asn133, and Asp58. (iii) The target oxidation site of HCB is attacked by flavin-N5-

peroxide. Since HCB lacks electron withdrawing groups to resonantly stabilize the anion intermediate, the negative charge is temporarily stabilized by the benzene ring, and the target chlorine atom subsequently leaves as a chloride ion, producing an FMN-substrate hydroperoxide intermediate. His17, within hydrogen bonding distance from the oxygen atom that is covalently bonded to the target carbon atom, is proposed to coordinate these intermediates. (iv) Deprotonation of the FMN-substrate hydroperoxide gives a flavin-N5-oxide and a hydroxyl product PCP. (v) Reduction of the flavin-N5-oxide by NADH and elimination of water regenerate the starting oxidized FMN.

It is also noteworthy that this N5-oxygenation mechanism may be more widespread than commonly appreciated, especially in the bacterial luciferase family. These enzymes may have been overlooked in the flavin biochemical literature because their detailed catalytic and substrate-selective mechanism has yet to be further elucidated. Therefore, investigating flavin-N5-peroxide-utilizing enzymes, not only bacterial ones but also those from archaea, plants, and animals, is anticipated to broaden our understanding of flavoenzymes.

Future applications. Viewed from an environmental angle, the investigations into the dechlorinases of chloro-organic pollutants are far from adequate. As far as we know, among the 19 compounds of POPs, only the dechlorinases of DDT, chlordecone, and hexachloro-cyclohexane have been structurally studied (43, 44). Through our data, the structural and biochemical study laid a foundation for the rational design of HcbA1 to obtain variants with desired substrate specificity and improved enzyme activity, which will be hopefully employed for the initial oxidative attack of HCB or other chloro-organic compounds in chemical industry and environmental biotechnology applications.

MATERIALS AND METHODS

Cloning, expression, and purification. Gene fragments of , , and were synthesized by the Nanjing Yidao Biotechnology Co. Wild-type , , and , and mutants of , were cloned into pET-28a(+) (Novagen, USA) and expressed in BL21(DE3)- (kindly provided by Luying Xun of Washington State University). Cells were grown at 37°C until the optical density at 600 nm (OD_{600}) reached 0.6, and then 0.2 mM isopropyl-β-D-thiogalactopyranoside (IPTG) was used to induce protein expression at 16°C for a further 12 h.

Cells were harvested, washed, and then resuspended in buffer A (50 mM Tris-HCl [pH 7.8], 300 mM NaCl, 1 mM dithiothreitol [DTT], 5% glycerol). After disruption by sonication, supernatant was obtained by centrifugation for 60 min at 32,000 × and applied onto a preequilibrated Ni^{2+}-chelating affinity column. The target protein was eluted with buffer A supplemented with 250 mM imidazole. Proteins were further purified using a Superdex-200 gel filtration chromatography column (GE Healthcare Life Sciences, Pittsburgh, USA) and then ultrafiltered to the required concentration for subsequent catalytic analysis and crystallization.

Enzyme activity assay and kinetic measurement. The enzymatic activity was determined based on its capability of degrading HCB, and the consumed amount of HCB was calculated by measuring the residual HCB concentration. In each group of experiments, the reaction solution without NADH was used as a negative control and was treated exactly as the experimental group to calculate the spike recovery. A standard curve of HCB, with its concentrations ranging from 5 to 100 μM (diluted from a stock solution of 1 mM HCB–acetone), exhibited a good linearity. A standard enzyme assay mixture contained 5.4 μM HcbA1, 0.056 μM HcbA3, 30 μM HCB, 0.3 mM NADH, and 0.02 mM FMN in 300 μl (final volume) of Tris-HCl buffer (50 mM, pH 7.8). Protein concentration was determined by the Bradford method with bovine serum albumin as a standard. HCB was quantified by HPLC after extraction of 0.3 ml of the reaction mixture with 0.3 ml of ethyl acetate. One unit of enzyme activity was defined as the amount required for the disappearance of 1 μmol of HCB per min at 30°C. Specific activities were expressed as units per gram of protein. The kinetic parameters were determined in the same reaction mixture as described above, with the HCB concentration ranging from 5 to 100 μM. Kinetic data were evaluated by nonlinear regression analysis performed with the Michaelis-Menten equation $\{v = _{max} \times [S]/(+ [S])\}$, using the Windows-based program GraphPad Prism 5.0.

The effect of reaction temperature on HCB monooxygenase activity was monitored between 15°C and 55°C in Tris-HCl buffer (pH 8.0). The effect of pH on its enzymatic activity was also determined using 50 mM citrate buffer (pH 3.0 to 6.0), 50 mM MES (morpholineethanesulfonic acid) buffer (pH 5.5 to 7.0), 50 mM HEPES buffer (pH 6.5 to 8.0), 50 mM Tris-HCl (pH 7.5 to 9.0), and 50 mM glycine buffer (pH 8.5 to 10.0).

Analytical methods. The concentration of HCB was monitored by the use of an HPLC system (Waters Alliance 2695, USA) equipped with a UV detector (set at 216 nm), using a Poroshell 120 EC-C_{18} column (Agilent Technologies, Tokyo, Japan) at 30°C. The mobile phase was 90:10 acetonitrile–0.1% phosphoric acid, and the pump was set to run in isocratic mode with a flow rate of 1.0 ml/min. The retention times of HCB and PCP were 10.3 min and 4.4 min, respectively, using the conditions listed above. Assays of the

trapped intermediate PCP were performed by derivatization with acetic anhydride to pentachlorophenyl acetate prior to detection (18). Gas chromatography-mass spectrometry (GC-MS) analysis was carried out using an Agilent 6850/5975C system and a DB-5 fused silica capillary column (0.32-mm inner diameter by 30 m by 0.25 μm) and previously published methods (43). The injection volume was 1 μl, and splitless injection was used. The retention times of HCB and PCP were 20.08 min and 21.56 min, respectively. The protein conformations of HcbA1 and its mutants were evaluated by CD (JASOC, Japan; model CD/J-815) in the near-UV region (250-nm to 320-nm wavelength).

Crystallization and structure determination. HcbA1 was subjected to buffer exchange into a mixture containing 10 mM Tris-HCl (pH 7.8), 50 mM NaCl, and 5% glycerol, and the reaction mixture was concentrated to 7.0 mg/ml by ultrafiltration. Crystals were grown using the sitting-drop vapor-diffusion method at 20°C by mixing equal volumes of protein solution and reservoir solution. The reservoir solution contained 0.1 M Bis-Tris (pH 5.5) and 1.8 M $(NH_4)_2SO_4$. Diffraction-quality crystals of HcbA1 appeared within 6 days. The crystals of the HcbA1-FMN complex were obtained by adding 1.4 mM FMN to the protein solution before crystallization. The aforementioned crystals were soaked in a reservoir solution with 20% glycerol as a cryoprotectant and flash cooled in liquid nitrogen for data collection. Data were collected at 100 K on the BL19U beamline at the Shanghai Synchrotron Radiation Facility. All X-ray diffraction intensity data were integrated, scaled, and merged using the program HKL3000 (45). For structure determination, the phasing problem was solved by molecular replacement performed with the program Phaser in the CCP4 program suite (46). LadA from [illegible] NG80-2 (PDB entry 3B9N) (28), which shares 38% sequence identity with HcbA1, was employed as a search model. The programs COOT (47) and Phenix (48) were used for manual adjustment and refinement of the model, respectively. An [illegible] substrate docking procedure was performed using AutoDock Vina (49). The HcbA1·FMN structure was used as a search template for the substrate-binding poses.

MD simulations. The parameters of FMN and HCB were generated at the HF/6-31G(d) level of theory with the Gaussian 09 program (50). The restrained electrostatic potential (RESP) (51) charge fitting procedure was employed for FMN and HCB, and missing parameters were generated by the Antechamber package. The complex was solvated with a 10-Å buffer of TIP3P water, and sodium ions were added to neutralize the system.

MD simulations were run using the AMBER software package (version 18) (52). The enzymes and substrates were described by ff12SB and GAFF force fields from the AMBER18 software package. The Particle mesh Ewald (PME) (53) method was used for long-range electrostatic interactions. In addition, the SHAKE algorithm was employed to fix angles and bonds involving hydrogen atoms (54). Prior to production of MD simulations, solvated systems were treated with heating and minimization steps, with the system temperature increasing from 0 to 298 K over 50 ps. After equilibration for 50 ps, a 50-ns production simulation was carried out on the complexes without any restraints under NPT (number of

We thank the staff of beamline BL19U1 of the National Center for Protein Science Shanghai (China) for access and help with the X-ray data collection and the staff of the Instrumental Analysis Center of Shanghai Jiao Tong University for the technical assistance.

We declare that we have no conflicts of interest with the contents of this article.

REFERENCES

1. Antunes P, Viana P, Vinhas T, Rivera J, Gaspar EM. 2012. Emission profiles of polychlorinated dibenzodioxins, polychlorinated dibenzofurans (PCDD/Fs), dioxin-like PCBs and hexachlorobenzene (HCB) from secondary metallurgy industries in Portugal. Chemosphere 88:1332–1339. https://doi.org/10.1016/j.chemosphere.2012.05.032.
2. Starek-Świechowicz B, Budziszewska B, Starek A. 2017. Hexachlorobenzene as a persistent organic pollutant: toxicity and molecular mechanism of action. Pharmacol Rep 69:1232–1239. https://doi.org/10.1016/j.pharep.2017.06.013.
3. Ahmed G, Anawar HM, Takuwa DT, Chibua IT, Singh GS, Sichilongo K. 2015. Environmental assessment of fate, transport and persistent behavior of dichlorodiphenyltrichloroethanes and hexachlorocyclohexanes in land and water ecosystems. Int J Environ Sci Technol 12:2741–2756. https://doi.org/10.1007/s13762-015-0792-3.
4. Jones KC, de Voogt P. 1999. Persistent organic pollutants (POPs): state of the science. Environ Pollut 100:209–221. https://doi.org/10.1016/s0269-7491(99)00098-6.
5. Robles-Molina J, Gilbert-López B, García-Reyes JF, Molina-Díaz A. 2014. Monitoring of selected priority and emerging contaminants in the Guadalquivir River and other related surface waters in the province of Jaén, South East Spain. Sci Total Environ 479–480:247–257. https://doi.org/10.1016/j.scitotenv.2014.01.121.
6. Ye X, Dong F, Lei X. 2018. Microbial resources and ecology - microbial degradation of pesticides. Nat Resour Conserv Res 1:247–257.
7. Fathepure BZ, Tiedje JM, Boyd SA. 1988. Reductive dechlorination of hexachlorobenzene to tri- and dichlorobenzenes in anaerobic sewage sludge. Appl Environ Microbiol 54:327–330. https://doi.org/10.1128/AEM.54.2.327-330.1988.
8. Holliger C, Schraa G, Stams AJ, Zehnder AJ. 1992. Enrichment and properties of an anaerobic mixed culture reductively dechlorinating 1,2,3-trichlorobenzene to 1,3-dichlorobenzene. Appl Environ Microbiol 58:1636–1644. https://doi.org/10.1128/AEM.58.5.1636-1644.1992.
9. Chang BV, Su CJ, Yuan SY. 1998. Microbial hexachlorobenzene dechlorination under three reducing conditions. Chemosphere 36:2721–2730. https://doi.org/10.1016/s0045-6535(97)10231-4.
10. Wu Q, Milliken CE, Meier GP, Watts JE, Sowers KR, May HD. 2002. Dechlorination of chlorobenzenes by a culture containing bacterium DF-1, a PCB dechlorinating microorganism. Environ Sci Technol 36:3290–3294. https://doi.org/10.1021/es0158612.
11. Liu T, Chen Z, Shen Y. 2009. Aerobic biodegradation of hexachlorobenzene by an acclimated microbial community. Int J Environ Pollut 37:235–244. https://doi.org/10.1504/IJEP.2009.025127.
12. Gopalakrishnan J, Görisch H, Adrian L. 2003. Dehalorespiration with hexachlorobenzene and pentachlorobenzene by sp. strain CBDB1. Arch Microbiol 180:411–416. https://doi.org/10.1007/s00203-003-0607-7.
13. Takagi K, Iwasaki A, Kamei I, Satsuma K, Yoshioka Y, Harada N. 2009. Aerobic mineralization of hexachlorobenzene by newly isolated pentachloronitrobenzene-degrading sp. strain PD653. Appl Environ Microbiol 75:4452–4458. https://doi.org/10.1128/AEM.02329-08.
14. Ito K, Takagi K, Kataoka R, Kiyota H, Iwasaki A. 2019. Dissipation, dehalogenation, and denitration of chloroaromatic compounds by sp. strain PD653: characterization of the substrate specificity. J Pestic Sci 44:171–176. https://doi.org/10.1584/jpestics.D19-024.
15. Adrian L, Rahnenführer J, Gobom J, Hölscher T. 2007. Identification of a chlorobenzene reductive dehalogenase in sp. Strain CBDB1. Appl Environ Microbiol 73:7717–7724. https://doi.org/10.1128/AEM.01649-07.
16. Jones JP, O'Hare EJ, Wong LL. 2001. Oxidation of polychlorinated benzenes by genetically engineered CYP101 (cytochrome P450(cam)). Eur J Biochem 268:1460–1467. https://doi.org/10.1046/j.1432-1327.2001.02018.x.
17. Chen X, Christopher A, Jones JP, Bell SG, Guo Q, Xu F, Rao Z, Wong LL. 2002. Crystal structure of the F87W/Y96F/V247L mutant of cytochrome P-450cam with 1,3,5-trichlorobenzene bound and further protein engineering for the oxidation of pentachlorobenzene and hexachlorobenzene. J Biol Chem 277:37519–37526. https://doi.org/10.1074/jbc.M203762200.
18. Yan DZ, Liu H, Zhou NY. 2006. Conversion of ATCC 39723 to a hexachlorobenzene degrader by metabolic engineering. Appl Environ Microbiol 72:2283–2286. https://doi.org/10.1128/AEM.72.3.2283-2286.2006.
19. Ito K, Takagi K, Iwasaki A, Tanaka N, Kanesaki Y, Martin-Laurent F, Igimi S. 2017. Identification of the hcb gene operon involved in catalyzing aerobic hexachlorobenzene dechlorination in sp. Appl Environ Microbiol 83:e00824-17. https://doi.org/10.1128/AEM.00824-17.
20. Adak S, Begley TP. 2019. Hexachlorobenzene catabolism involves a nucleophilic aromatic substitution and flavin-N5-oxide formation. Biochemistry 58:1181–1183. https://doi.org/10.1021/acs.biochem.9b00012.
21. Xiao Y, Liu TT, Dai H, Zhang JJ, Liu H, Tang H, Leak DJ, Zhou NY. 2012. OnpA, an unusual flavin-dependent monooxygenase containing a cytochrome b(5) domain. J Bacteriol 194:1342–1349. https://doi.org/10.1128/JB.06411-11.
22. Ang T-F, Maiangwa J, Salleh A, Normi Y, Leow T. 2018. Dehalogenases: from improved performance to potential microbial dehalogenation applications. Molecules 23:1100. https://doi.org/10.3390/molecules23051100.
23. Banner DW, Bloomer AC, Petsko GA, Phillips DC, Pogson CI, Wilson IA, Corran PH, Furth AJ, Milman JD, Offord RE, Priddle JD, Waley SG. 1975. Structure of chicken muscle triose phosphate isomerase determined crystallographically at 2.5 angstrom resolution using amino acid sequence data. Nature 255:609–614. https://doi.org/10.1038/255609a0.
24. Huijbers MM, Montersino S, Westphal AH, Tischler D, van Berkel WJ. 2014. Flavin dependent monooxygenases. Arch Biochem Biophys 544:2–17. https://doi.org/10.1016/j.abb.2013.12.005.
25. Okai M, Lee WC, Guan LJ, Ohshiro T, Izumi Y, Tanokura M. 2017. Crystal structure of dibenzothiophene sulfone monooxygenase BdsA from WU-S2B. Proteins 85:1171–1177. https://doi.org/10.1002/prot.25267.
26. Kim SH, Hisano T, Takeda K, Iwasaki W, Ebihara A, Miki K. 2007. Crystal structure of the oxygenase component (HpaB) of the 4-hydroxyphenylacetate 3-monooxygenase from HB8. J Biol Chem 282:33107–33117. https://doi.org/10.1074/jbc.M703440200.
27. Krissinel E, Henrick K. 2007. Inference of macromolecular assemblies from crystalline state. J Mol Biol 372:774–797. https://doi.org/10.1016/j.jmb.2007.05.022.
28. Li L, Liu X, Yang W, Xu F, Wang W, Feng L, Bartlam M, Wang L, Rao Z. 2008. Crystal structure of long-chain alkane monooxygenase (LadA) in complex with coenzyme FMN: unveiling the long-chain alkane hydroxylase. J Mol Biol 376:453–465. https://doi.org/10.1016/j.jmb.2007.11.069.
29. Matthews A, Saleem Batcha R, Sanders J, Stull F, Houk K, Teufel R. 2020. Aminoperoxide adducts expand the catalytic repertoire of flavin monooxygenases. Nat Chem Biol 16:556–563. https://doi.org/10.1038/s41589-020-0476-2.
30. Campbell ZT, Weichsel A, Montfort WR, Baldwin TO. 2009. Crystal structure of the bacterial luciferase/flavin complex provides insight into the function of the beta subunit. Biochemistry 48:6085–6094. https://doi.org/10.1021/bi900003t.
31. Bissantz C, Kuhn B, Stahl M. 2010. A medicinal chemist's guide to molecular interactions. J Med Chem 53:5061–5084. https://doi.org/10.1021/jm100112j.
32. Imai YN, Inoue Y, Yamamoto Y. 2007. Propensities of polar and aromatic amino acids in noncanonical interactions: nonbonded contacts analysis of protein-ligand complexes in crystal structures. J Med Chem 50:1189–1196. https://doi.org/10.1021/jm061038a.
33. Lommerse JPM, Stone AJ, Taylor R, Allen FH. 1996. The nature and geometry of intermolecular interactions between halogens and oxygen or nitrogen. J Am Chem Soc 118:3108–3116. https://doi.org/10.1021/ja953281x.

34. Raman CS, Li H, Martásek P, Southan G, Masters BSS, Poulos TL. 2001. Crystal structure of nitric oxide synthase bound to nitro indazole reveals a novel inactivation mechanism. Biochemistry 40:13448–13455. https://doi.org/10.1021/bi010957u.
35. Holm L, Rosenstrom P. 2010. Dali server: conservation mapping in 3D. Nucleic Acids Res 38:W545–W549. https://doi.org/10.1093/nar/gkq366.
36. Tian M, Loidl J. 2018. A chromatin-associated protein required for inducing and limiting meiotic DNA double-strand break formation. Nucleic Acids Res 46:11822–11834. https://doi.org/10.1093/nar/gky968.
37. Meunier B, de Visser SP, Shaik S. 2004. Mechanism of oxidation reactions catalyzed by cytochrome p450 enzymes. Chem Rev 104:3947–3980. https://doi.org/10.1021/cr020443g.
38. Teufel R, Miyanaga A, Michaudel Q, Stull F, Louie G, Noel JP, Baran PS, Palfey B, Moore BS. 2013. Flavin-mediated dual oxidation controls an enzymatic Favorskii-type rearrangement. Nature 503:552–556. https://doi.org/10.1038/nature12643.
39. Saleem-Batcha R, Stull F, Sanders JN, Moore BS, Palfey BA, Houk KN, Teufel R. 2018. Enzymatic control of dioxygen binding and functionalization of the flavin cofactor. Proc Natl Acad Sci U S A 115:4909–4914. https://doi.org/10.1073/pnas.1801189115.
40. Adak S, Begley TP. 2016. Dibenzothiophene catabolism proceeds via a flavin-N5-oxide intermediate. J Am Chem Soc 138:6424–6426. https://doi.org/10.1021/jacs.6b00583.
41. Mukherjee T, Zhang Y, Abdelwahed S, Ealick SE, Begley TP. 2010. Catalysis of a flavoenzyme-mediated amide hydrolysis. J Am Chem Soc 132:5550–5551. https://doi.org/10.1021/ja9107676.
42. Adak S, Begley TP. 2017. RutA-catalyzed oxidative cleavage of the uracil amide involves formation of a flavin-N5-oxide. Biochemistry 56:3708–3709. https://doi.org/10.1021/acs.biochem.7b00493.
43. Chen L, Hall PR, Zhou XE, Ranson H, Hemingway J, Meehan EJ. 2003. Structure of an insect delta-class glutathione S-transferase from a DDT-resistant strain of the malaria vector . Acta Crystallogr D Biol Crystallogr 59:2211–2217. https://doi.org/10.1107/s0907444903018493.
44. Macwan AS, Kukshal V, Srivastava N, Javed S, Kumar A, Ramachandran R. 2012. Crystal structure of the hexachlorocyclohexane dehydrochlorinase (LinA-type2): mutational analysis, thermostability and enantioselectivity. PLoS One 7:e50373. https://doi.org/10.1371/journal.pone.0050373.
45. Minor W, Cymborowski M, Otwinowski Z, Chruszcz M. 2006. HKL-3000: the integration of data reduction and structure solution - from diffraction images to an initial model in minutes. Acta Crystallogr D Biol Crystallogr 62:859–866. https://doi.org/10.1107/S0907444906019949.
46. Winn MD, Ballard CC, Cowtan KD, Dodson EJ, Emsley P, Evans PR, Keegan RM, Krissinel EB, Leslie AG, McCoy A, McNicholas SJ, Murshudov GN, Pannu NS, Potterton EA, Powell HR, Read RJ, Vagin A, Wilson KS. 2011. Overview of the CCP4 suite and current developments. Acta Crystallogr D Biol Crystallogr 67:235–242. https://doi.org/10.1107/S0907444910045749.
47. Emsley P, Cowtan K. 2004. Coot: model-building tools for molecular graphics. Acta Crystallogr D Biol Crystallogr 60:2126–2132. https://doi.org/10.1107/S0907444904019158.
48. Liebschner D, Afonine PV, Baker ML, Bunkoczi G, Chen VB, Croll TI, Hintze B, Hung LW, Jain S, McCoy AJ, Moriarty NW, Oeffner RD, Poon BK, Prisant MG, Read RJ, Richardson JS, Richardson DC, Sammito MD, Sobolev OV, Stockwell DH, Terwilliger TC, Urzhumtsev AG, Videau LL, Williams CJ, Adams PD. 2019. Macromolecular structure determination using X-rays, neutrons and electrons: recent developments in Phenix. Acta Crystallogr D Struct Biol 75:861–877. https://doi.org/10.1107/S2059798319011471.
49. Trott O, Olson AJ. 2010. AutoDock Vina: improving the speed and accuracy of docking with a new scoring function, efficient optimization, and multithreading. J Comput Chem 31:455–461. https://doi.org/10.1002/jcc.21334.
50. Gaussian R, Trucks G, Schlegel H, Scuseria G, Robb M, Cheeseman J, Scalmani G, Barone V, Mennuci B, Petersson G, Nakatsuji H, Caricato M, Li X, Hratchian H, Izmaylov A, Bloino J, Zheng G, Sonnenberg J, Hada M, Fox D. 2004. Gaussian. Gaussian, Inc, Wallingford, CT.
51. Cornell W, Cieplak P, Bayly C, Gould I, Merz K, Ferguson D, Spellmeyer D, Fox T, Caldwell J, Kollman P. 1995. A second generation force field for the simulation of proteins. J Am Chem Soc 117:5179–5197. https://doi.org/10.1021/ja00124a002.
52. Case D, Ben-Shalom I, Brozell SR, Cerutti DS, Cheatham T, Cruzeiro VWD, Darden T, Duke R, Ghoreishi D, Gilson M, Gohlke H, Götz A, Greene D, Harris R, Homeyer N, Huang Y, Izadi S, Kovalenko A, Kurtzman T, Kollman PA. 2018. Amber 2018. https://iop.vast.ac.vn/theor/conferences/smp/1st/kaminuma/AMBER/index.htm.
53. Darden T, York DM, Pedersen LG. 1993. Particle mesh Ewald - an N.log(N) method for Ewald sums in large systems. J Comput Chem 18:1463–1472. https://doi.org/10.1063/1.464397.
54. Ryckaert J-P, Ciccotti G, Berendsen H. 1977. Numerical integration of Cartesian equations of motion of a system with constraints: molecular dynamics of n-alkanes. J Comput Phys 23:327–341. https://doi.org/10.1016/0021-9991(77)90098-5.
55. Roe D, Cheatham T. 2013. PTRAJ and CPPTRAJ: software for processing and analysis of molecular dynamics trajectory data. J Chem Theory Comput 9:3084–3095. https://doi.org/10.1021/ct400341p.
56. Humphrey W, Dalke A, Schulten K. 1996. VMD: visual molecular dynamics. J Mol Graphics 14:33–38. https://doi.org/10.1016/0263-7855(96)00018-5.